PII: S0955-2219(98)00171-X

0955-2219/98/$—see front matter

The Nuclear Microprobe in Materials Science: Application to Ceramics

P. Berger

Laboratoire Pierre SÜE, CEA/CNRS, CE/SACLAY, Gif sur Yvette, France

(Received 23 June 1997; accepted 4 July 1998)

Abstract

The aim of this paper is to present the analytical capabilities of the nuclear microprobe for the characterization of ceramics. The nuclear microprobe uses the interactions of a focused ion beam of MeV light ions (^1H, ^2H, ^3He, ^4He, ..) with a solid target to determine local elemental concentrations at the μm^3 scale. The main analytical techniques are based on the spectrometry of the induced X *and gamma-rays, and of the particles scattered or produced by nuclear reactions. Examples are shown such as concentration profiling of additives and dopants in alumina, oxygen-18 diffusion profiles and interfacial enrichment in nickel oxide scales grown under external mechanical loading, local oxygen stoichiometry and carbon contents in superconductor oxides, boron and carbon determination for local characterization in multiphase quaternary borocarbides.*

1 Introduction

The atomic and nuclear interactions of MeV light ions with a solid target have lead to the development of analytical techniques for surface or thin film characterization. Since the early sixties, like for the development of other analytical probes, the continuous trend have been to the decrease of the size of the ion beam, from millimeter to micron size. Since the lateral resolution of ion beam based measurements is directly connected to the size of the probe, the nuclear microprobe measures the microdistribution of the elements, sometimes 3-dimentional when depth profiling is possible.

In the MeV range, when penetrating a specimen, the great majority of the ions of the beam follows straight lines, losing gradually their energy by electronic interaction. A few of them are scattered by the nuclei and, for the closest impact parameters, nuclear reactions may occur on light nuclei.

The rate of energy loss, dE/dx, measured in units of MeV $(g\,cm^{-2})$, can be calculated from the weighted mean of the dE/dx values for the constituent elements with only very slight dependence on the chemistry (Bragg rule). As these stopping powers are known with a good accuracy (~3% for energies between 1 and 4 MeV), the nuclear microprobe gives reliable depth information.[1]

The first nuclear microprobe was built as early as 1969 at the Harwell research centre (UK).[2] The number of facilities is still increasing and nearly 60 nuclear microprobes are in operation all over the world. The nuclear microanalysis is applied to various fields such as solid state physics, metallurgy, geochemistry, life sciences, environmental science, archeology,.... In materials science, its ability to measure light elements by means of nuclear reactions is used for local elemental depth profiling or stoichiometry determinations.

The aim of this paper is to give an overview of the analytical capabilities of the nuclear microprobe for the characterization of oxides and ceramics. One of the most important feature of the nuclear microprobe is that it produces a wide variety of different analytical signals which can be combined together. We will present the basic principle of single techniques and a few examples which associate two or more different signals.

2 Particle Induced X-ray Emission (PIXE)

Like for the X-ray emission induced by electron bombardment, when an atom is excited or ionized by the ions of the beam, the relaxation of inner-shell vacancies leads to the emission of X-rays characteristic of the elements, in the 1–30 keV range.[3] Compared to the electrons, the ions induce much smaller bremsstrahlung radiation background, because of the higher mass of the ions. As a consequence, the elemental sensitivity of PIXE is then usually enhanced by a factor 10–100.[4]

Figures 1(a) and (b) show the spectra obtained on an Al_2O_3 sample doped with calcium, for 20 keV electrons and 3 MeV protons, respectively. The reduction of the background under the bombardment of the protons enhances the Kα line intensity of the calcium (note that the choice of 3 MeV was driven by the need of multielemental analysis, 1 MeV being a better choice for the sensitivity on calcium determination).

For 3 MeV protons, the maximum sensitivity is obtained for two ranges of atomic numbers, $25 < Z < 35$ and $75 < Z < 85$, corresponding to the maximum of the cross-sections of inner-shell ionization for K and L levels.[4]

The energy spectrum of the X emission can be treated by means of simulation programs which enable to unfold the signals from all the elements above $Z = 10$ in the specimen, although interferences by major elements can sometimes severely limit the sensitivity for detecting particular trace elements. The GUPIX software is one of the most popular.[5]

PIXE is by far the most used technique for nuclear microprobe measurements, but rather for biological applications than for materials science. The high sensitivity of the method enables the reduction of the local density of ions when a high lateral resolution is required (i.e. with a beam size from 1 μm to a few 100 nm), especially for high resolution X-ray imaging. Although developed for the determination of trace elements, the PIXE may be also used for the major and minor elements, in association with the others ion beam techniques.

X-spectra do not contain depth information but the analyzed depth depends mainly on the energy of the photons (from within a μm to a few 10 μm). Assuming the homogeneity of the sample, a specific depth might be probed by the choice of the energy

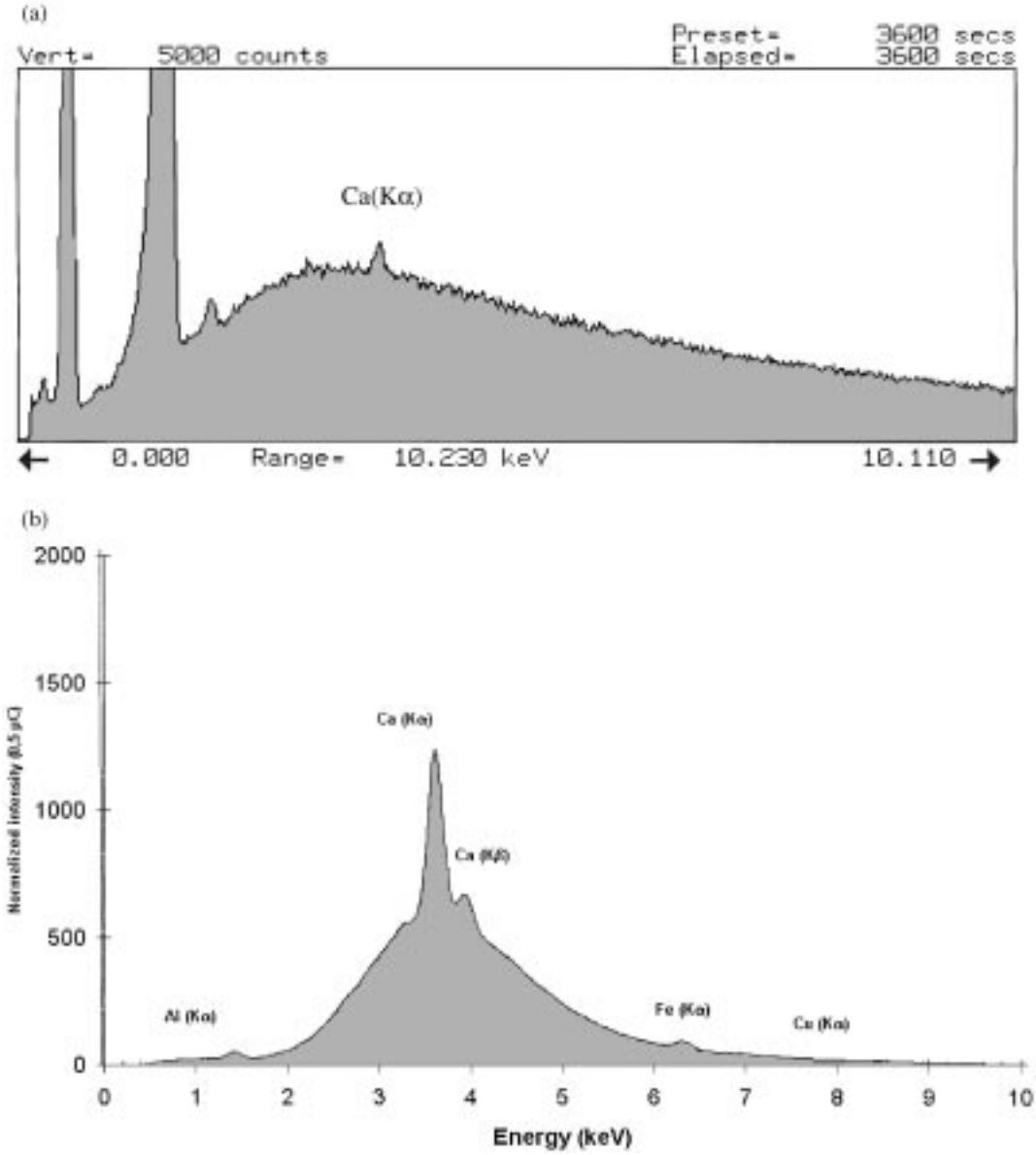

Fig. 1. (a) X-ray spectrum induced on calcium doped alumina by 20 keV electrons. (b) X-ray spectrum induced on calcium doped alumina by 3 MeV protons.

of the ions of the beam. The main features of PIXE are summarized in Table 1.

Figure 2 shows an example of the use of PIXE for a line scan of a stacked sample of doped Al_2O_3. The layers alternate different doping elements and the relative concentrations of the impurities range from minor to trace levels. In order to study the influence of these doping elements and additives on the grain growth rate and anisotropy during the sintering process, investigations on the microstructure have been correlated to their concentration levels. The concentration profile has been measured with an unfocussed beam ($\sim$40 $\times$ 50 μm^2) in order to get a mean concentration on several grains of the alumina.[6]

3 Elastic Scattering

The scattering of light ions by the coulomb repulsion of a nucleus is the basis of a family of techniques among which the Rutherford Backscattering (RBS) is the most used for its accuracy and simplicity.[7]

An ion scattered at backward angle loses more of its energy in a collision on a light nucleus than on an heavy one. The energy spectrum of the backscattered ions then allows the identification of the mass of the nuclei of the target. For thick targets, because of the energy loss of the ions entering and leaving the sample, the energy spectrum is continuous. Depth information may be extracted from the energy shift from the surface steps.

The analyzed thickness and depth resolution are related to the energy loss of the ions. The higher the loss, the higher the resolution. So, the performances of RBS depend on the nature of the target, on the nature of the ions and on their energy. Depth resolutions in the order of a few 10 nm may be achieved with ^4He beams, but rather a few 100 nm with protons because of their lower energy loss (cf. Table 1).

Table 1. Overview of the main features of ion beam based analytical methods

Method	*Field of application*	*Probed depth* (μm)[a]	*Depth resolution* (*nm*)[a]	*Sensitivity* (*wt ppm*)
PIXE (particle induced X-ray emission)	Trace and major elements (Na to U)	0·1–20	500–10^3	1–100
RBS (Rutherford backscattering spectrometry)	Thin films. Heavy elements	10^{-3}–10	15–30	100–10^3
PESA (particle enhanced scattering analysis)	Light element (Li to Si)	10^{-2}–10^{-1}	$\sim$ a few nm	10^3–10^4
ERDA (elastic recoil spectrometry)	Hydrogen isotopes	10^{-1}–10	20–40	10–100
NRA (nuclear reaction analysis)	Light element (H toS)	10^{-1}–10	5–500	1–10^3
PIGE (particle induced gamma-ray emission)	Minor and minor element (li to Ga)	10–50	500–10^3	100–10^3

[a]The probed depth and depth resolutions are related to the energy losses of the ions. According to the nature and to the energy of the ions, these quantities may vary from several orders of magnitude.

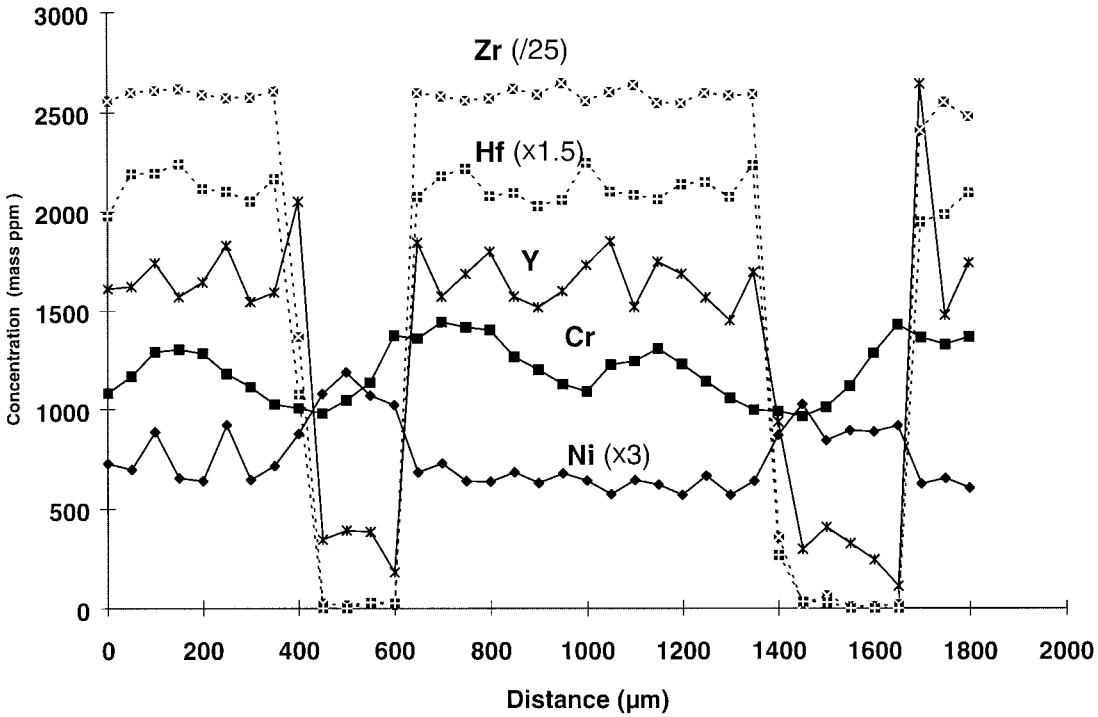

Fig. 2. PIXE longitudinal concentrations profiles measured on an alternate doped stacked alumina sample.

As the cross-sections of RBS are proportional to the square of the atomic number of the elements, the sensitivity is high for the heaviest (a few 100 ppm) but low for the lightest. Fortunately, resonances and enhanced elastic scattering may occur for some values of the energy of the incident ion (PESA for Particle Enhanced Scattering Analysis), depending on its nature and related to the nuclear structure of light elements from He to Si. These cross-sections are 1–3 orders of magnitude higher than Rutherford ones.[8–10]

For instance, the use of a $^4He^+$ beam allows the combination of RBS for the analysis of the cations and resonant scattering for the oxygen, by means of the $^{16}O(\alpha,\alpha)^{16}O$ resonance at 3·045 MeV. The maximum cross-sections of this resonance are about 15 times higher than Rutherford cross-sections. Since the sensitivity on oxygen is greatly enhanced, a whole elemental composition may be determined in a single measurement. Used with a microbeam, RBS mapping allows to seek for possible lateral heterogeneities or local stoichiometries.

Figure 3(a) and (b) shows a typical spectrum and an example of mapmaking, obtained with 3·05 MeV $^4He^+$ on a thin film of a superconducting

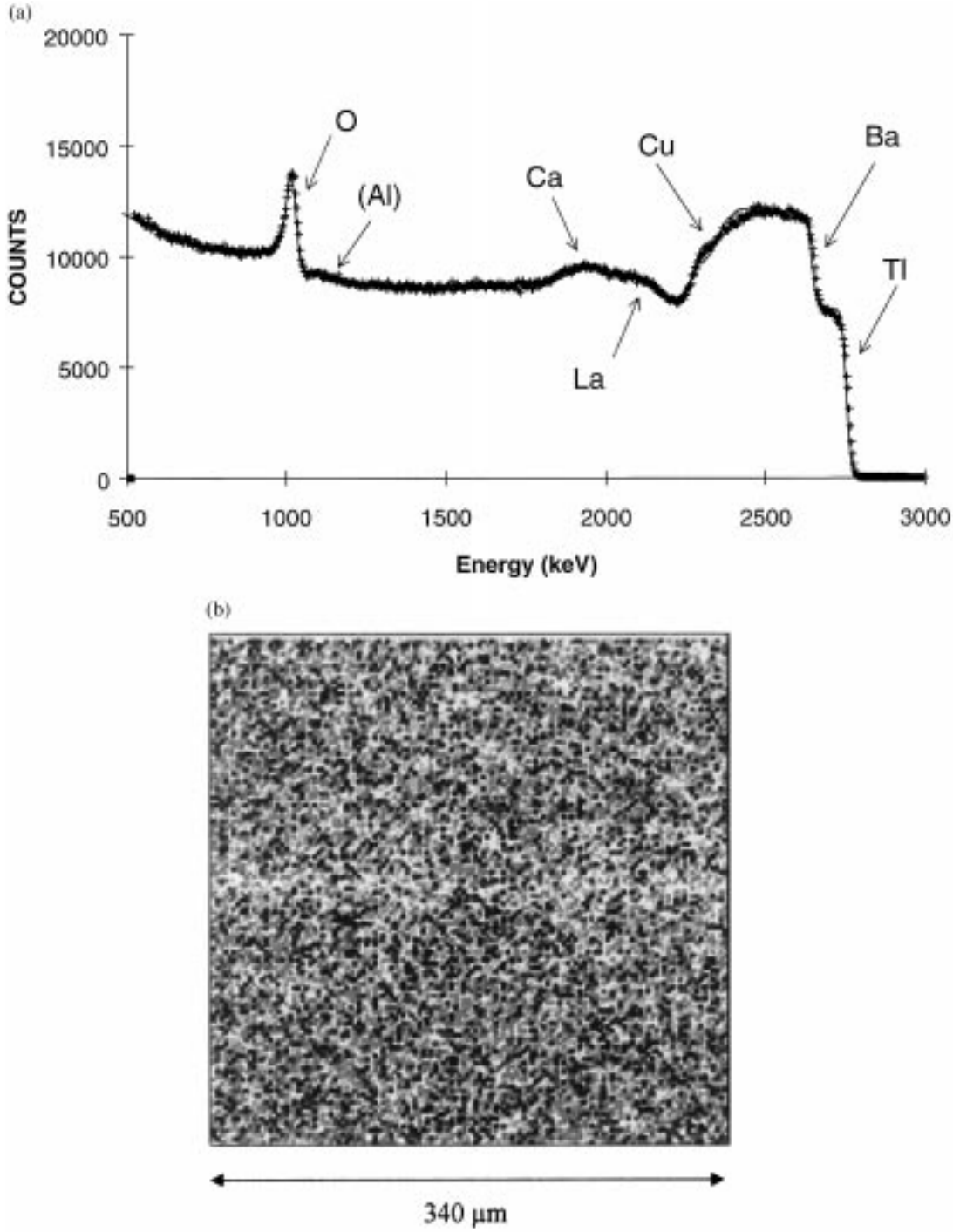

Fig. 3. (a) RBS spectrum on a $Tl_2Ba_2CaCu_2O_8$ superconducting film deposited on $LaAlO_3$. (b) RBS map of thallium.

oxide $Tl_2Ba_2CaCu_2O_8$ deposited on a single crystal of $LaAlO_3$.[11] These films are obtained by *ex situ* oxygen annealing of precursor amorphous films, deposited at room temperature with a multitarget sputtering system. The rapid loss of thallium by volatilization of thallium oxide represents one of the major difficulties for obtaining pure phases from the precursor film.

The superconducting film is about 6000–7000 Å thick. Since the 3·045 MeV resonance is narrow (10 keV), the $^4He^+$ ions of the beam reach the energy of the resonance at the top of the film only (~2000Å). When they reach $LaAlO_3$, as they have lost a sufficient amount of energy, the helium ions no longer induce enhanced scattering on oxygen. It enables to measure the oxygen content in the film without interference with the oxygen of the substrate.

The spectrum of Fig. 3(a) has been measured by scanning the $^4He^+$ microbeam on an area of 340 × 340 μm^2. The matrix of Fig. 4(b) has been constructed by selecting an energy window in the

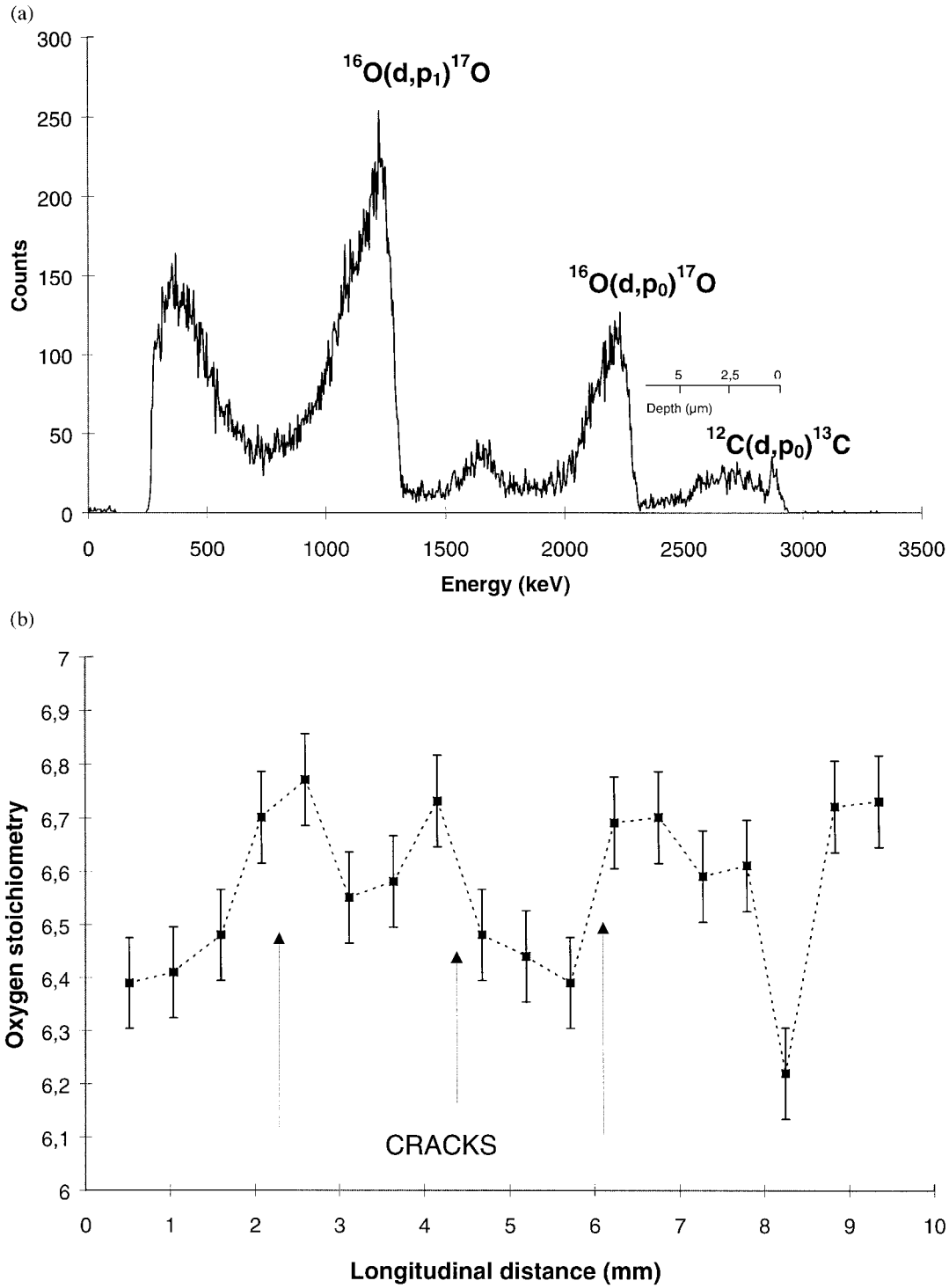

Fig. 4. (a) NRA spectrum of protons induced by 1·4 MeV ^2H on YBaCuO. (b) Longitudinal scan of oxygen stoichiometry in a non-reoxygenated textured YBaCuO sample.

spectrum at the thallium step. Each pixel corresponds to the integral of the counts recorded in this window for each individual position of the beam (128×128 points with a microbeam of $2{\cdot}5\times2{\cdot}5\,\mu m^2$). The spectrum of a selected zone within the scanned area may be also reconstructed by selecting given pixels only.

The RUMP program package[12] has been used for data reduction by simulation and fit of the spectra. Within the same area, the film is rather homogeneous, but long distance lateral heterogenities of the composition have been observed from one zone to another. However, despite these stoichiometric variations, the sample has been found always fully oxygenated.

A variation of the methods based on elastic scattering is the Elastic Recoil Detection Analysis (ERDA) where the recoil nucleus is detected after its collision with the incident ion. ERDA is currently applied for hydrogen profiling in solids using 2–4 MeV $^4He^+$ ions. Detection limits of the order of 50–100 ppm may be attained with a microbeam.[13]

4 Nuclear Reaction Analysis (NRA)

This technique relies on the detection of charged particles, neutrons or gamma-rays emitted in nuclear reactions. The inelastic collisions between the ions of the probe and the light nuclei of the target lead to the formation of new nuclei, usually with emission of particles differing from the incident ions.

To induce a nuclear reaction, the incident ion must have enough energy to overcome the coulomb barrier of the target nucleus. The higher the atomic number, the higher the barrier is. Although the energy of the ions of the microprobe is limited to a few MeV, the light elements from hydrogen to sulfur may be analyzed with isotopic selectivity.[8,9,14,15]

As most of the reactions used for microanalysis are exoenergetic, the emitted particles from nuclear reactions usually carry higher energies than the incident ions. These particles may then be distinguished from the backscattered ones. In some cases, a mylar foil is inserted before the detector to stop all the backscattered while the nuclear reaction induced particles undergo partial slowing down only.

Like for the elastic scattering, the energy spectrum of the emitted particles may be converted into depth profile, but the depth resolution is often slightly lower ($\geqslant 50$ nm) because of their lower energy loss (cf. Table 1). Sometimes, an increase of the depth resolution (5–10 nm) may be obtained by the use of resonances with a strong increase of the cross-sections for a very narrow energy window, practically in the order of a few keV.

When a nucleus produced by nuclear reaction is left on an excited state, the relaxation to its fundamental state induces the emission of characteristic gamma-ray, ranging from a few hundred keV to several MeV according to the nature of the nucleus. The spectrometry of these gamma rays, (PIGE for Particle Induced Gamma Ray Emission), is a sensitive method but has a poor depth resolution and suffers from interferences in multielemental samples.[8,9,16]

The low cross-sections of nuclear reactions, in comparison to PIXE or RBS, restrain the use of NRA microbeam mapping. But, for the determinations of stoichiometry, spot measurements give reliable data on multiphase samples, containing one or more light elements. To give an example, quaternary borocarbides in the NiReBC (Re = Rare Earth) and YPdBC systems form complex compounds whose physical properties, superconductivity and magnetism, depend strongly on the composition of minor phases.[17] To try to identify the ≪active≫ phases in the microstructure, the local simultaneous determination of the concentrations of boron and carbon may be done with a microbeam of ^3He. The nuclear reactions induced by ^3He ions are highly exoenergetic and the spectra have a complex structure due to the great number of nuclear levels involved. But, as the nuclear reactions induced on boron isotopes are much more energetic than those induced on carbon, the individual contribution of each of them may be easily unfolded. Thus, by a combination, in a single measurement, of RBS to determine the cation stoichiometry and NRA for the carbon and boron, it has been shown that in the multiphase $YPd_5B_3C_{0{\cdot}35}$, the superconducting phase had a composition close to YPd_2B_2C.[18]

Another example may be shown for the characterization of YBaCuO superconductor oxides. The dependence of the critical temperature on the oxygen stoichiometry of bulk samples is well-known, but the seek for new synthesis routes needs often local investigations to reveal the presence of lateral heterogeneities, diffusion short-circuits or barriers. Deuteron induced nuclear reactions allow the simultaneous measurement of oxygen and carbon.[19] The Fig. 4(a) shows a typical proton spectrum from induced reactions $^{16}O(d,p_0)^{17}O$, $^{16}O(d,p_1)^{17}O$ and $^{12}C(d,p_0)^{13}C$ on an YBaCuO superconductor oxide. The local oxygen concentration may be obtained from the p_1 group by comparision to a reference sample and stopping power calculations, practically independent of the chemical state. The determination of the oxygen

stoichiometry needs to know the cation stoichiometry which may be deduced from the induced X-rays spectrum, simultaneouly collected.

An advantage of the simultaneous measurement of the carbon content from the $^{12}C(d,p_0)^{13}C$ nuclear reaction is to avoid an overestimation of the oxygen stoichiometry due to the presence of carbonates (synthesis residus, atmospheric surface reactivity). In addition, as the proton spectrum is depth resolved, one can distinguish bulk carbon content from surface corrosion or contamination. In principle, the oxygen depth distribution may be checked also. But, as only small variations of the oxygen content are expected, the counting statistics do not allow to evidence abnormal depth profiles.

The simultaneous measurement of the gamma spectrum give an intense peak near 871 keV emitted from the ^{17}O nuclei produced by the $^{16}O(d,p_x)^{17}O$ nuclear reactions. Although not depth resolved, the PIGE technique is likely to give the best precision ($\sim$1%) for oxygen stoichiometry determinations in locally homogeneous zones.[20]

Figure 4(b) shows a longitudinal scan of the oxygen stoichiometry measured with a deuteron beam on a textured YBaCuO, before the reoxygenation step (needed for the adjustment of the superconductive properties). Significant variations may be observed and high oxidation zones seem to be correlated with the presence of cracks in the microstructure of the sample.[21]

A third example of the use of nuclear reactions may be found in the study of oxygen diffusion in NiO scales grown on stressed samples.[22,23] To investigate the influence of an external loading on the growth of nickel oxide, monocrystalline nickel samples have been mounted in a tensile machine placed into an oven under controlled atmosphere $^{16}O_2/^{18}O_2$. The growth is performed in 3 steps: a former ^{16}O oxidation without load, a second oxidation under a constant load (a few 10 MPa) and a final run under ^{18}O.

The oxide scales grown during creep tests show periodic cracking with the cracks perpendicular to the strain axis (cf. Fig. 5). The distance between cracks depends on the intensity of the load, but the mean wideness of the stripes is in the order of 10 μm.

Accurate oxygen-18 profiles have to be measured either above stripes or across cracks. This may be done with a 600–800 keV proton beam by means of the nuclear reaction $^{18}O(p,\alpha)^{15}N$.[24] Figure 6 shows the energy spectrum of the a ions induced by 780 keV protons on a stripe of the most heavily loaded (60 MPa) nickel (100) sample. As, in this energy range, the variations of the cross-sections of the reaction are small, the intensity of the signals is nearly proportional the concentration. Stopping

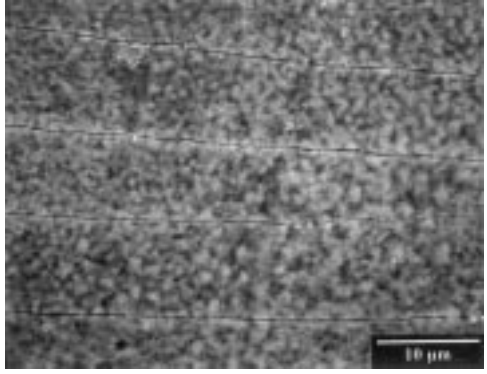

Fig. 5. SEM micrograph of the NiO scales grown during creep tests.

power calculations enable to convert the energy scale in a depth scale. Although the ^{18}O has been introduced at the end of the run, a significant ^{18}O enrichment occurs at the oxide/metal interface. These diffusion short-circuits are not observed for lower loadings.

5 Channeling and Other Analytical Techniques

For a crystalline sample, the ions may be channelled along some peculiar directions of the beam with respect to the sample. The modifications of the yield of backscattered particles or X-ray emission give quantitative information about the lattice disorder, the location of impurity atoms in the lattice sites, or the composition and thickness of amorphous surface layers.[25]

Experiments on YBaCuO or BiSrCaCuO monocrystals have been held at the Oxford nuclear microprobe with proton beams, on twinned crystals to reveal the presence of strain due to the twin structure (cf. Fig. 7), and on Fe-substituted crystals to investigate the location of Fe with respect to the Cu position in the lattice.[26–28]

Practically, the lateral resolution of microchanneling is limited to a few tens of microns because of the damage built-up induced by the ion beam itself during the measurement.[29]

The recent developments of nuclear microprobe techniques concern mainly the imaging of thin samples (from 1 to a few 10 μm). The Scanning Transmission Ion Microscopy (STIM) is based on the spectroscopy of energy losses of the incident ions,[30] sometimes in channeling conditions (CSTIM).[31] As nearly all the incident particles are detected, only very low currents are required ($\sim 10^{-15}$ A) which allows high lateral resolution ($\sim$50 nm) and induces low damaging. Although its performances are significantly lower than the transmission electron microscopy, the STIM technique enables the investigation of thicker samples.

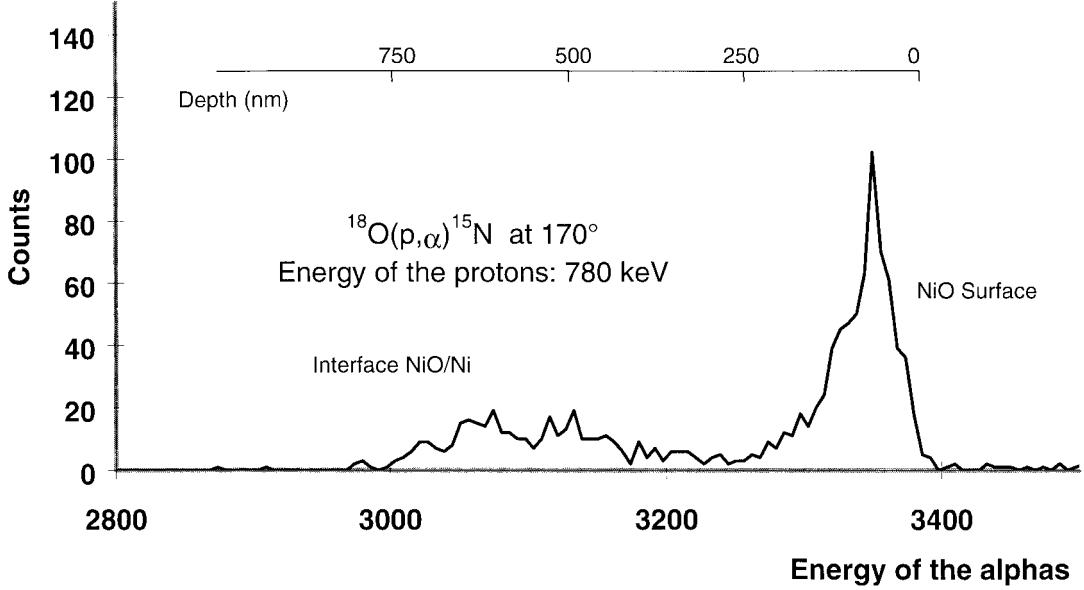

Fig. 6. NRA spectrum of α ions induced by 780 keV protons on NiO scales after $^{18}O_2$ treatment.

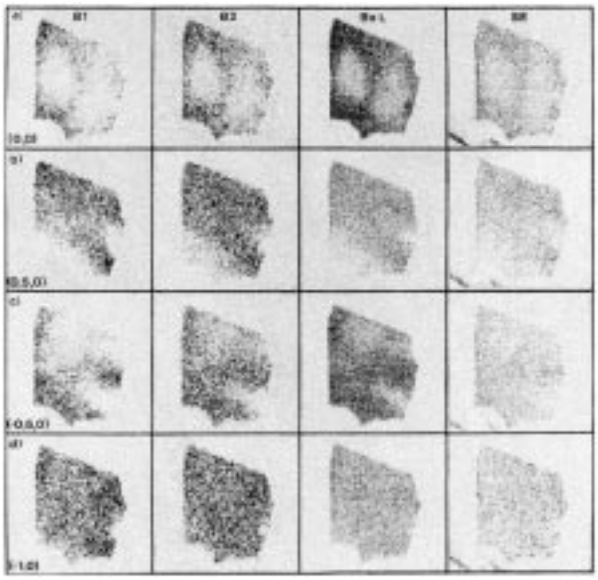

Fig. 7. Channeling with a 2×2 μm^2 2 MeV proton beam on a single crystal of YBaCuO. The columns correspond respectively to the backscattered protons at shallow depth and deeper, to the X-ray from baryum (Kα lines) and to the secondary electrons. The rows correspond to different misorientations between the beam axis and the (001) direction (from Ref. 26).

The CSTIM technique have been applied to the study of imaging of colomnar structures in 3C-SiC thin films deposited on silicon,[32] and to the imaging of stacking faults on Si wafers about 10 μm below the surface of samples that are several tens of microns in thickness.[33]

6 Conclusion

Because of the limited number of laboratories operating MeV ion microbeams, ion beam based microanalytical techniques are not extensively used in materials science. Although one may find higher performance techniques when either elemental sensitivity, lateral or depth resolution are required, the nuclear microprobe has the ability to perform the three at once with a high accuracy on elemental concentrations or depth measurements. The measurements on the light elements by means of nuclear reactions with isotopic selectivity is probably its most original feature.

In order to improve the access to these techniques, the nuclear microprobe of the Pierre SÜE laboratory works as a national facility.

References

1. Anderson, N. N. and Ziegler, J. F., *Stopping Powers and Ranges in All Elements*. Pergamon Press, New York, 1977.
2. Cookson, J. A., Ferguson, A. T. G. and Pilling, F. D., Proton microbeams, their production and use. *J. Radioanal. Chem.*, 1972, **12**, 39–52.
3. Folkmann, F., Ion induced X-rays, general description. In: *Materials Characterization Using Ion Beams*, ed. J. P. Thomas and A. Cachard, Plenum Press, New York, 1978.
4. Johansson, S. A. E. and Campbell, J. L., *PIXE, A Novel Technique for Elemental Analysis*. John Wiley, Chichester, 1988.
5. Campbell, J. L., Teesdale, W. J. and Maxwell, J. A., Practical problems with a proton probe. *Nucl. Inst. and Meth.*, 1991, B56/57, 694–698.
6. Suenaga, K. *et al.*, Microstructure of polycrystalline alternate doped alumina stacked layers. *Proceedings of ECRS-V*, Versailles, June 22–26, 1997.
7. Chu, W. K., Mayer, J. W. and Nicolet, M. A., *Backscattering Spectrometry*. Academic press, New York, 1978.
8. Mayer, J. W. and Rimini, E., *Ion Beam Handbook for Materials Analysis*. Academic press, New York, 1977.
9. Bird, J. R. and Williams, J. S., *Ion Beam Handbook for Materials Analysis*. Academic press, Sidney, 1990.
10. Tessmer, J. R. and Nastasi, M., *Handbook of Modern Ion Beam Materials Analysis*. Materials Research Society, Pittsburg, 1995.

11. Gasser, C. *et al*., $Tl_2Ba_2CaCu_2O_8$ superconducting thin films: a comparative study of ex Situ annealing using amorphous precursors with different thallium content. *J. Solid State Chem*., 1996, **121**, 262–272.
12. Doolittle, L. R., Semi automatic algorythm for Rutherford backscattering spectrometry. *Nucl. Inst. and Meth*., 1986, **B15**, 227–231.
13. Tirira, J., Serruys, Y. and Trocellier, P., *Forward Recoil Spectrometry: Applications to Hydrogen Determination in Solids*. Plenum Press, New York, 1996.
14. Deconninck, G., *Introduction to Radioanalytical Physics*. Elsevier, Amsterdam,1978.
15. Demortier, G., Analysis of light elements with a nuclear microprobe—a review. *Nucl. Inst. and Meth*, 1995, **B104**, 244–254.
16. Borderie, B., Present possibilities for bulk analysis in prompt gamma-ray spectrometry with charged particles. *Nucl. Inst. and Meth*., 1980, **175**, 465–482.
17. Godart, C. *et al*., Structural superconductivity and magnetic properties of YNi2B2C ErNi2B2C. *Phys. Rev*., 1995, **B51**, 489–496.
18. Tominez, E. and Berger, P. *et al*., On the 22-23K superconducting phase in the Y-Pd-B-C system. *Journal of Alloys and Compounds*, 1998, **275–277**, 123–126.
19. Demortier, G. *et al*., Stoichiometric characterisation of Y-Ba-Cu-O superconductors with nuclear probes. *Nucl. Inst. and Meth*., 1988, **B30**, 491–496.
20. Vickridge, I., Tallon, J. and Presland, M., High precision determination of ^{16}O in high Tc superconductors by DIGME . *Nucl. Inst. and Meth*., 1994, **B85**, 95–99.
21. Berger, P. *et al*., Nuclear microprobe local characterization of YBaCuO superconductors. *Nucl. Inst. and Meth*., 1995, **B104**, 542–546.
22. Moulin, G., Arevalo, P. and Salleo, A., Influence of external mechanical loadings (creep, fatigue) on oxygen diffusion during nickel oxidation. *Oxid. met*., 1995, **45**, 10–17.
23. Moulin, G. and Berger, P., Interaction between oxidation and deformation in the case of nickel in creep at 550°C. *Mat. Sci. Forum*, 1996, **207**, 809–812.
24. Berger, P., Moulin, G. and Viennot, M., Nuclear microprobe study of stress-oxidation of nickel. *Nucl. Inst. and Meth*. 1997, **B270**, 717–721.
25. Ingarfield, S. A. *et al*., Semiconductor analysis with a channeled helium microbeam. *Nucl. Inst. and Meth*., 1981, **191**, 521–526.
26. Romano, L. T. *et al*., Channeling nuclear microscopy of $Y_1Ba_2Cu_3O_{7-\delta}$ single crystal. *Nucl. Inst. and Meth*., 1991, **B54**, 234–238.
27. Romano, L. T. *et al*., Atomic position of Fe in $YBa_2(Cu_{1-x}Fe_x)_3O_{7-\delta}$ using channeling. *Phys. Rev*., 1991, **B44**, 6927–6931.
28. Lee, K. K. *et al*., Nuclear microscopy of Fe substituted 2212 BiSrCaCuO superconducting crystals. *Nucl. Inst. and Meth*., 1995, **B104**, 561–565.
29. Jamieson, D. N. *et al*., Applications of MeV ion microbam to the analysis of single-crystal materials. *Nucl. Inst. and Meth*., 1991, **B54**, 213–224.
30. Bench, G. S. and Legge, G. J. F., High resolution STIM. *Nucl. Inst. and Meth*., 1989, **B40/B41**, 655–658.
31. Cholewa, M. *et al*., Channeling scanning transmission ion microscopy. *Appl. Phys. Lett*., 1990, **56**, 1236–1238.
32. Sekiguchi, H. *et al*., Study of 3C-SiC crystal defects by micrbeam channeling methods. *Nucl. Inst. and Meth*., 1995, **B104**, 566–570.
33. King, P. J. C. *et al*., Application of transmission ion channeling to the imaging of stacking faults. *Nucl. Inst. and Meth*., 1995, **B104**, 233–237.